https://doi.org/10.5194/egusphere-2025-5159
Preprint. Discussion started: 3 December 2025

A nine-year record of slush on the Greenland Ice Sheet

Emily Glen[1,2], Alison F. Banwell[3,4], Katie E. Miles[1], Amber A. Leeson[1,2], Rebecca L. Dell[5], Malcolm McMillan[1,2], Jennifer Maddalena[1,2]

[1] Lancaster Environment Centre, Lancaster University, Lancaster, UK
[2] Centre for Polar Observation and Modelling, Lancaster University, Lancaster, UK
[3] Cooperative Institute for Research in Environmental Sciences (CIRES), University of Colorado Boulder, Boulder, USA
[4] Centre for Polar Observation and Modelling, School of Geography and Natural Sciences, Northumbria University, Newcastle Upon Tyne, UK
[5] Scott Polar Research Institute, University of Cambridge, Lensfield Road, Cambridge, UK

Correspondence to: Emily Glen (e.glen@lancaster.ac.uk)

Abstract. Surface melt on the Greenland Ice Sheet (GrIS) has intensified in recent decades, accelerating GrIS mass loss. Slush (i.e., water-saturated firn or snow) is a key component of this system, yet its areal extent and behaviour remains poorly constrained. Here, we present the first GrIS-wide classification of slush, using over 300,000 Sentinel-2 images and a supervised Random Forest classifier in Google Earth Engine. We generate a nine-year (2016–2024), high spatial resolution (10 m) dataset, which we then use to perform an ice sheet wide systematic assessment of slush distribution across all six major drainage basins. On average, slush covers ~2.9% (~50,400 km²) of the entire GrIS each summer, with around 40% (~29,300 km²) of this area in regions with low-permeability ice slabs or by firn aquifers. Slush shows marked interannual variability that mirrors variability in melt intensity, ranging from a maximum slush areal extent of 1.2% (20,500 km²) of the ice sheet in 2018, the lowest melt year of the time series, to a maximum of 5.2% (90,300 km²) in 2019, the highest melt year. When our results are evaluated alongside those from other studies, we find that slush is the dominant meltwater feature in terms of spatial coverage on the GrIS each melt season: the maximum slush area was nine and four times greater than the combined area of supraglacial lakes and streams in 2019 and 2018, respectively. As climate change drives more frequent and prolonged extreme melt seasons on the GrIS, slush is likely to increase in area. Given the influence of slush on lateral meltwater transport, firn-air depletion, and melt–albedo feedback, its incorporation into energy balance and hydrological models will help better constrain ice-sheet mass balance projections.

1. Introduction

The Greenland Ice Sheet (GrIS) has experienced a negative mass balance for several decades, losing ice at a rate of −255 ± 19 Gt yr^{-1} from 2002 to 2022 (Otosaka et al., 2023). Supraglacial melting and runoff are the principal drivers of this mass loss, accounting for ~70% of total ice sheet mass loss between 2007 - 2012 (IMBIE, 2020). Between 1991–2019, the mean summer air temperature on the GrIS increased by ~1.7°C (Hanna et al., 2021), contributing to a 21% increase in supraglacial runoff between 2011 and 2020 compared to the previous three decades (Slater et al., 2021; Trusel et al., 2018). Superimposed on this

https://doi.org/10.5194/egusphere-2025-5159
Preprint. Discussion started: 3 December 2025

long-term warming trend are increasingly frequent extreme melt events (Bonsoms et al., 2024); short-lived episodes of anomalously intense melting typically driven by persistent high-pressure systems (Tedesco and Fettweis, 2020). In response to both long-term warming and an increase in the frequency of extreme melt events, supraglacial meltwater features, particularly lakes, have expanded in both area and elevation over recent decades (Fan et al., 2025; Leeson et al., 2015; Howat et al., 2013), with the maximum elevation of runoff shifting inland by up to 329 m a.s.l. in elevation between 1985 and 2020 (Tedstone and Machguth, 2022). In some regions, melt now reaches far into the percolation zone, areas that historically experienced little or no seasonal melting (Tedesco, 2007; Fettweis et al., 2011), creating conditions favourable for the formation of slush, which we define here as fully water-saturated firn or snow (Cogley et al., 2011).

Slush, first observed during early Greenland expeditions in the early twentieth century and formally described by Holmes (1955), typically forms in the percolation zone when vertical drainage is impeded, either by a low permeability ice layer or by saturation of the firn pore space, which waterlogs the overlying firn and snow. Holmes (1955) distinguished between surface slush and subsurface slush. Surface slush is fully saturated at the surface and can be detected in optical satellite imagery (referred to as blue slush), whereas sub-surface slush is overlain by an unsaturated snow (referred to as white slush) and therefore cannot be identified in optical imagery (Greuell and Knap, 2000; Machguth et al., 2022. Once slush forms, the reduced vertical permeability causes meltwater to be preferentially routed laterally This process enhances surface hydrological connectivity, as meltwater flows more readily through slush than through dry snow and firn (Clerx et al., 2022), feeding supraglacial rivers and lakes (Holmes, 1955). Slush can act as a precursor to supraglacial channelisation, either through directing excess meltwater into topographic depressions where channel incision is initiated (Chu, 2014; Rippin and Rawlins, 2021), or through removal of the previous winter's snow from an existing channel (Tedesco et al., 2013). These channels can link to moulins or crevasses, providing a pathway through which meltwater can be routed to the ice-sheet bed (Tedesco et al., 2013; Banwell et al., 2013; 2016) thereby promoting basal lubrication and dynamic ice loss (e.g., de Fleurian et al., 2018; Koziol and Arnold 2018). Upon refreezing, slush has the potential to thicken pre-existing near-surface ice slabs (Tedstone et al., 2025). These multi-metre-thick bodies of refrozen ice can extend over tens of kilometres (Machguth et al., 2016; MacFerrin et al., 2019) and, due to their low permeability, restrict vertical meltwater transport and storage, enhancing runoff from inland areas (Machguth et al., 2016; Tedstone and Machguth, 2022; Culberg et al., 2024).

Despite its hydrological importance, slush remains largely absent from large-scale meltwater mapping efforts across the GrIS. Only a limited number of studies have attempted to quantify the areal extent and/or elevation of slush, either through catchment-scale mapping of its spatial distribution (e.g., Covi et al., 2022; Rawlins et al., 2023; Glen et al., 2025) or - at larger spatial scales - by identifying the 'runoff limit', defined as the highest elevation where visibly saturated firn or snow is present in satellite imagery (Gruell and Knap, 2000; Tedstone and Machguth, 2022; Machguth et al., 2023). Recent observations suggest that both the elevation and areal extent of slush are highly sensitive to interannual melt variability. For example, within the Watson catchment, southwest Greenland, slush was found to cover a substantially larger area and extend to higher

https://doi.org/10.5194/egusphere-2025-5159
Preprint. Discussion started: 3 December 2025

elevations during the extreme melt year of 2019 compared to the below-average melt year of 2018 (Glen et al., 2025), increasing from ~1.6% of the catchment (~80 km²) in 2018 to 7.6% (~380 km²) in 2019, and expanding upslope from elevations below 1,500 m to above 1,800 m. Similarly, long-term satellite analyses indicate a systematic upward migration of the runoff limit, with Landsat imagery revealing a 29% increase in elevation between 1985 and 2020 (Tedstone and Machguth, 2022), and MODIS imagery detecting slush at elevations approaching ~2080 m a.s.l. in western Greenland (Machguth et al., 2023).

Recent findings from Antarctic ice shelves further emphasise the importance of slush within polar ice sheet hydrological and mass balance systems more generally. Dell et al. (2024) show that slush accounts for approximately 50% of the total meltwater area across 57 ice shelves, suggesting that previous meltwater inventories – focused primarily on supraglacial lakes and channels – significantly underestimate total meltwater storage in Antarctica. Given the climatological similarities between Antarctic ice shelves and the percolation zone of the GrIS, it is reasonable to hypothesize that similar findings may apply to Greenland as well. Dell et al. (2024) demonstrate that incorporating slush processes into regional climate models - especially via the positive melt-albedo feedback from surface saturation (e.g. Banwell et al., 2023) - nearly triples modeled snowmelt. Fully accounting for slush in ice sheet meltwater budgets and climate models is therefore crucial to better estimate surface melt and runoff, both now and into the future.

Here, we adapt a machine learning (ML) workflow developed for Antarctic ice shelves (Dell et al., 2022; 2024) to classify surface slush (henceforth *'slush'*) across the entire GrIS using Sentinel-2 imagery in Google Earth Engine (GEE). This represents the first application of ML to map slush on the GrIS, through which we generate an ice-sheet-wide dataset of slush extent spanning nine years (2016–2024). Using these data, we analyse spatial and temporal patterns across all six major drainage basins, and characterise ice-sheet-wide distribution, interannual variability, elevation patterns, and the relative importance of slush within the GrIS' broader meltwater regime.

2. Methods and data

To date, the majority of remote sensing studies of ice sheet surface meltwater have focused on supraglacial lakes and channels, which are meltwater features with relatively distinct spectral characteristics and well-defined boundaries. Therefore, compared to slush, these features can be mapped with reasonable accuracy using threshold-based methods, such as the Normalised Difference Water Index adapted for ice ($NDWI_{ice}$) (e.g., Williamson et al., 2017, 2018; Miles et al., 2017). Slush has diffuse boundaries and a muted blue hue in optical imagery, making it difficult to isolate using standard thresholding techniques. In such approaches, slush is typically either omitted entirely (classified as 'non-water') or included within broader 'water' classes without being distinguished from lakes or channels, leading to underestimation or mischaracterisation of its extent (e.g., Rawlins et al., 2023; Yang and Smith, 2012).

https://doi.org/10.5194/egusphere-2025-5159
Preprint. Discussion started: 3 December 2025

Random Forest (RF) algorithms (e.g., Dirscherl et al., 2020; Dell et al., 2022; 2024) and deep learning methods (e.g., Qayyum et al., 2020; Dunmire et al., 2025) have recently shown promise as an alternative to image thresholding for meltwater classification in both Greenland and Antarctica. For slush specifically, Dell et al. (2022, 2024), employed a k-means clustering approach to generate training classes from Landsat 8 imagery, which were then used to train an RF classifier to identify slush (and supraglacial water bodies) on Antarctic ice shelves. However, no study has yet applied ML classification methods such as these specifically for slush detection on the GrIS.

Here, we classify slush on the GrIS by following the approach outlined by Dell et al. (2022, 2024), but with adaptations for application to the GrIS, as detailed in the following sections and Figure 1. We conduct our analysis across all six basins of the GrIS: Southwest (SW), Central West (CW), Northwest (NW), North (NO), Northeast (NE) and Southeast (SE) (Fig. 2; Mouginot and Rignot, 2019).

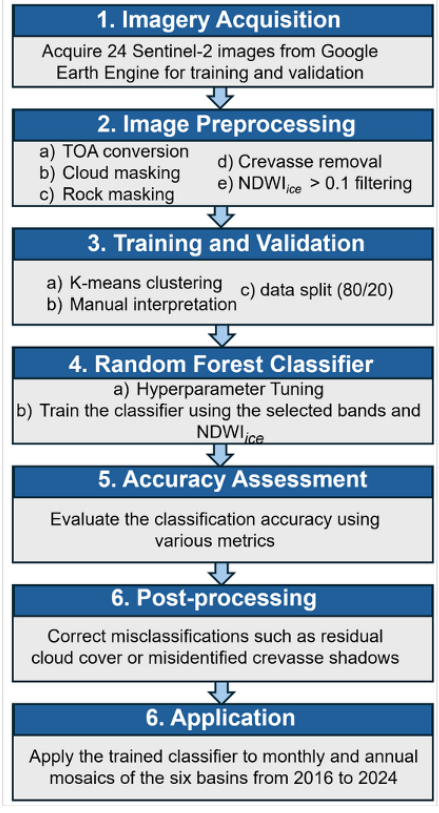

Figure 1: Flowchart of slush classification methodology adapted from Dell et al. (2022; Antarctic ice shelves) for application to the GrIS in this study.

https://doi.org/10.5194/egusphere-2025-5159
Preprint. Discussion started: 3 December 2025

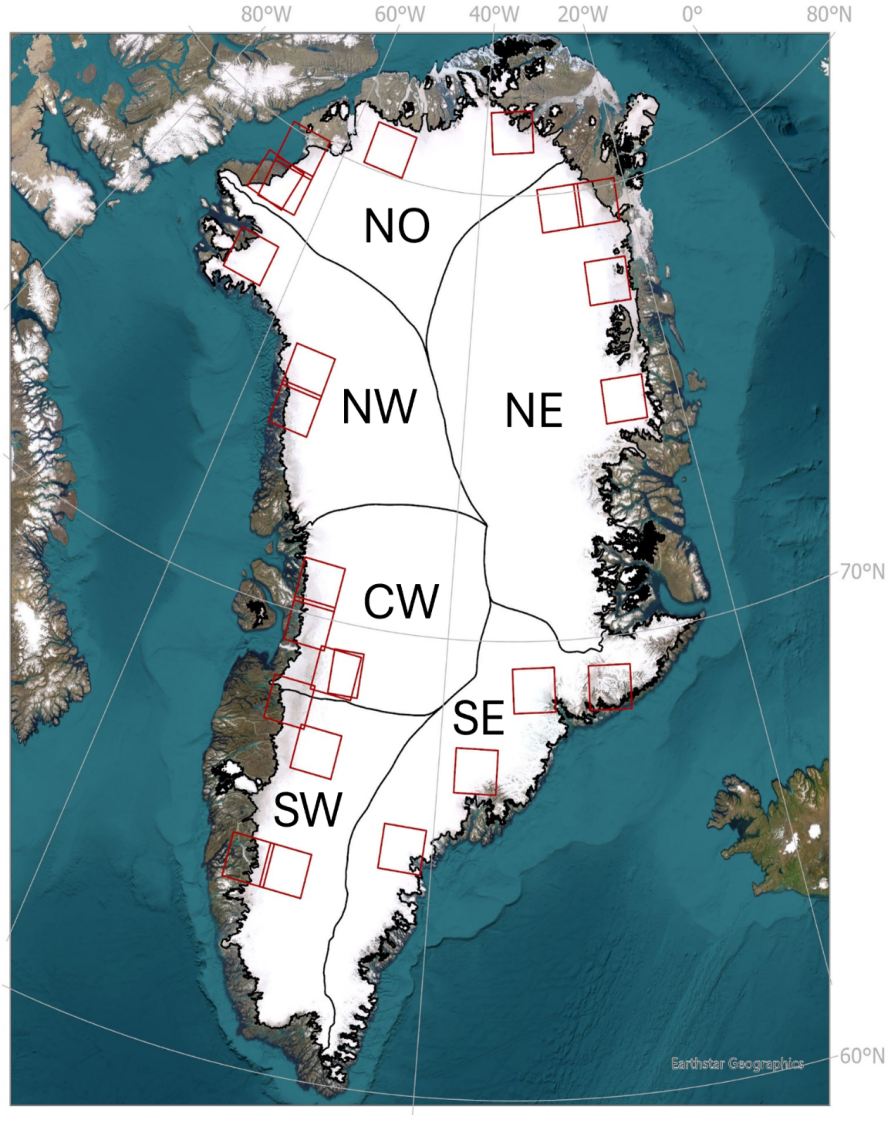

Figure 2: Overview map of the GrIS separated into six drainage basins: SW, CW, NW, NO, NE and SE (Mouginot and Rignot, 2019). Red boxes indicate footprints of the 24 training/validation images used to train and validate the RF classifier used in this study. Base map source: Esri.

https://doi.org/10.5194/egusphere-2025-5159
Preprint. Discussion started: 3 December 2025

2.1. Data

2.1.1. Sentinel-2 imagery

We acquired and pre-processed Level-1C Sentinel-2 (S2) MultiSpectral Instrument (MSI) imagery from the European Space Agency (ESA) via the GEE data catalogue, processing a total of 329,229 images from May to September, 2016 to 2024. Images were converted to Top-of-Atmosphere reflectance using a scaling factor of 10,000 (ESA, 2015). To improve meltwater feature detection, we restricted the dataset to scenes with a solar elevation angle > 20° (Halberstadt et al., 2020) and cloud cover < 25%. All available MSI bands were used in the analysis.

2.1.2. Supporting datasets

We used the 2 m ArcticDEM mosaic (Porter et al., 2023) to provide high-resolution surface topography across the ice sheet. The ArcticDEM is used to mask crevassed areas following Chudley et al. (2020) as well as to determine the maximum elevation of slush. For the latter, ArcticDEM elevations were sampled every 500 m along the upper limit of mapped slush across the ice sheet and averaged to estimate the maximum slush elevation.

Ice slab extents were taken from Jullien et al. (2023), who used airborne accumulation radar data collected across the Greenland Ice Sheet between 2002 and 2018 to map spatial variations in ice slab extent and thickness. We use their "high-end" estimates of slab extent in our analysis. Firn aquifer extents were taken from Miège et al. (2016), who identified widespread aquifers using NASA Operation IceBridge accumulation radar flown during five airborne campaigns between 2010 and 2014.

Melt and air temperature data were obtained from the Regional Atmospheric Climate Model RACMO2.3p2 (Noël et al., 2019). RACMO provides monthly 2 m air temperature and surface melt at 5.5 km spatial resolution, statistically downscaled to 1 km (Noël et al., 2018, 2019). Melt and temperature anomalies were calculated relative to the 1958–2015 monthly climatology for each summer month (May–September) and for each year between 2016 and 2024. These anomaly datasets were used to characterise interannual variability in melt and near-surface air temperature during our study period.

2.2 Image pre-processing

2.2.2. Image masking

To mask confounding surface features, we applied a cloud-detection algorithm based on thresholds from Corr et al. (2022), adding a 1 km buffer to account for cloud shadows. Rock outcrops were excluded using a modified Normalised Difference Snow Index (NDSI; Moussavi et al., 2020), also buffered by 1 km to ensure complete removal. A crevasse mask, derived from 2 m ArcticDEM data (Porter et al., 2023), was used to remove crevasses to prevent misclassification errors (Chudley et al., 2021).

https://doi.org/10.5194/egusphere-2025-5159
Preprint. Discussion started: 3 December 2025

Meltwater features, including slush, were then isolated using an $NDWI_{ice}$ (equation 1) threshold, which is a variant of the 'standard NDWI' (McFeeters, 1996). While the standard NDWI, calculated from the green (B3) and near-infrared (B8) bands, is best for terrestrial environments and, in some cases, ice sheet surfaces (e.g. Box and Ski, 2007), $NDWI_{ice}$ is specifically optimised for ice and firn surfaces and instead uses the blue (B2) and red (B4) bands (Yang and Smith, 2012).

$$NDWI_{Ice} = \frac{B2-B4}{B2+B4} \quad (1)$$

While Dell et al. (2022) applied a > 0.1 $NDWI_{ice}$ threshold for Antarctic ice shelves, we increased this to > 0.12 for Greenland (Yang and Smith, 2012) to account for regional differences in surface albedo and reflectance. Additionally, we used a blue band reflectance threshold of > 0.03 to filter out shadows cast by rocks, crevasses, and other non-meltwater features (Dirscherl et al., 2020; Corr et al., 2022).

2.2.3. Mosaic creation

Monthly and annual S2 mosaics were generated for each basin over the period 2016–2024 (May–September). After image filtering and masking, all available S2 images were combined into mosaics using the *qualityMosaic* function in GEE, which retains the maximum $NDWI_{ice}$ value for each pixel across overlapping images to capture the strongest meltwater signal in a given month or year (Dell et al., 2022). These monthly and annual mosaics were then used as the input datasets for the RF classifier (Section 2.4)

2.3. Label generation for model training and validation

For each GrIS drainage basin (Fig. 2), we manually selected four S2 images (24 images in total across all basins) for training and validation (Table S1). Images were chosen from the 2016–2024 melt seasons (1 May to 30 September) and selected to capture spectral variability by representing a range of solar elevation angles (42°–75°) and both high- and low-melt conditions. All images were clipped to the boundaries of the six drainage basins (Fig. 2).

Following pre-processing, residual non-meltwater elements such as faint cloud shadows and crevasse artefacts were manually removed through visual inspection to ensure only meltwater features were retained for analysis. Although the proportion of features requiring manual correction could not be quantified, such instances were infrequent and typically limited to small, spectrally ambiguous areas in regions with complex topography.

Training and validation data were derived from the 24 pre-processed S2 images using k-means clustering, following the approach of Halberstadt et al. (2020) and Dell et al. (2022). This method combines automated clustering with manual interpretation, which can reveal spectral patterns that may be overlooked in manual labelling alone. The k-means algorithm

https://doi.org/10.5194/egusphere-2025-5159
Preprint. Discussion started: 3 December 2025

grouped pixels based on spectral characteristics using all S2 bands as well as the $NDWI_{ice}$. For each image, 100,000 pixels were sampled and 5 to 70 clusters were generated (Dell et al., 2022).

Clusters were manually reviewed to identify 'slush,' defined as dense, light blue patches in true-colour S2 image composites, versus 'non-slush,' which included all other surface types (e.g., supraglacial lakes, channels, shadows, sediment, cryoconite), with any residual masked surfaces (e.g., rock, cloud, crevasses) also incorporated into the 'non-slush' class. Clusters that could not be confidently assigned to either class were excluded. From the remaining clusters, an equal number of pixels (2,000 per class) were randomly selected to create a balanced dataset, which was then randomly split into 80% for training and withheld 20% for validation.

2.4. RF model training and validation

Following Dell et al (2022), the classification of slush from S2 satellite imagery was performed using a RF classifier, implemented within GEE (ee.Classifier.smileRandomForest). This is an ensemble learning method that trains multiple decision trees on random subsets of data and features and classifies by majority voting (Breiman, 2001). In this study, the RF classifier was applied to all S2 bands as well as the $NDWI_{ice}$ band (Dell et al., 2022).

Unlike Dell et al. (2022), who used default settings, we optimised RF hyperparameters through an iterative tuning approach, systematically varying one parameter at a time and evaluating validation accuracy across each parameter range (Fig. S2). Parameters tested included the number of trees, bag fraction, minimum leaf population, maximum nodes, and random seed. Validation accuracies were compared across configurations, and the optimal setup was selected based on the highest observed accuracy. The final model used 50 trees, a bag fraction of 0.7, and a minimum leaf population of 20, with full details provided in Table S2.

2.4.1. Model performance

We evaluated performance of the RF classifier using the withheld 20 % validation dataset (Fig. S3; Table S3). Confusion matrices provided overall accuracy, the Kappa statistic (κ), F1-scores, precision, and recall. Commission errors occur when non-slush pixels are incorrectly classified as slush (false positives), while omission errors occur when true slush pixels are missed by the classifier (false negatives). The classifier achieved high performance (overall accuracy = 97.5%, $\kappa = 0.85$), with strong F1-scores for both slush (98.6%) and non-slush (86.4%). In terms of the number of misclassified pixels, 1,133 non-slush pixels were labelled as slush and 1,000 slush pixels labelled as non-slush, indicating a slight tendency of the RF classifier to overpredict slush (Fig. S3).

https://doi.org/10.5194/egusphere-2025-5159
Preprint. Discussion started: 3 December 2025

2.5. Application of trained RF model

Once trained, the supervised RF classifier was applied across all six drainage basins (Fig. 2) to the monthly and annual S2 image mosaics acquired between 2016 and 2024 (Section 2.1.3).

As in previous studies (e.g., Corr et al., 2022), manual post-processing was carried out to correct obvious misclassifications, including removal of areas of residual cloud cover and shaded areas near crevasses and fjords. Approximately 5–7% of pixels in each final mosaic were identified as misclassified and removed from the dataset. Our mosaicing approach ensured consistent monthly coverage across the record, and no year was disproportionately affected by cloud or temporal gaps. This strengthens confidence that the enhanced slush extents observed in high-melt years, for example, reflect genuine surface conditions rather than artefacts of reduced cloud cover (e.g., Hofer et al., 2017).

2.6. Comparison of the trained RF model to thresholding methods

We compared a subset of our RF slush classification results to those using two threshold-based methods: an NDWI approach combining both the standard NDWI and the $NDWI_{ice}$ (Glen et al., 2025) and a Greenness Index (Gind; Covi et al., 2022). Across test regions (i.e. one S2 image per basin over the nine years), RF showed stronger agreement with NDWI than with Gind, with higher overlap areas and F1-scores (0.56–0.76 vs. 0.53–0.65). Visual inspection confirmed these trends: NDWI aligned well with RF but was more prone to cloud contamination, while Gind often underdetected slush and misclassified lake edges. RF consistently produced more spatially coherent outputs, particularly when complex surface types with high variability in spectral characteristics were present. Full details of this analysis, including evaluation metrics, visual examples and details regarding the limitations of our classifier, are presented in the Supplement (Section S1; Fig. S1).

3. Results

3.1. Mean spatial distribution and persistence of slush from 2016-2024

Between 2016 and 2024, slush was detected across all six drainage basins of the GrIS (Fig. 3), with a mean summer (May–September) areal extent of ~2.9% (50,400 km²) of the ice sheet. The highest concentrations of slush typically occurred 10–20 km inland (Fig. 3), but slush was observed as far as 170 km inland during the most extreme melt year; 2019 (Fig. 4c).

Although slush was observed in every basin, its spatial coverage varied across the ice sheet (Fig. 3). Between 2016 and 2024, the SW basin exhibited the greatest proportional coverage (11,550 km²; 5.5% of its basin area), followed by the NO basin (11,660 km²; 4.8%), NE basin (14,590 km²; 3.0%), CW basin (4,430 km²; 1.9%), and NW basin (5,010 km²; 1.8%). The SE basin showed the lowest areal extent of slush (1,730 km²; 0.6%).

https://doi.org/10.5194/egusphere-2025-5159
Preprint. Discussion started: 3 December 2025

Slush persistence, defined as the number of melt seasons in which slush was detected at a given location, was examined on an interannual basis. Persistence was found to be highest in the NE and NO basins, where slush reappeared in the same locations during four out of nine melt seasons, whereas slush persistence was moderate in the NW and SW basins (three years) and lowest in the CW and SE basins (two years) (Fig. 3).

Considering the area of slush across the ice sheet as a whole, slush covered 149,660 km² (~9% of the ice sheet) in at least once melt season between 2016 and 2024, whereas only 1,671 km² (~0.1% of the ice sheet) was persistently slush in each and every one of the nine melt seasons. The basins that had the largest areas of this highly persistent slush (i.e. with slush present in every melt season) were the NE and NO, with 920 km² and 490 km², respectively. In the SW basin, despite having one of the highest mean slush areal extents over the nine-year period (11,550 km²), only 51 km² of this area was persistent slush in every melt season. The SE basin experienced both the lowest mean slush areal extent (1,730 km²) and the smallest area in which slush reoccurs in the same location in every melt season (43 km²).

https://doi.org/10.5194/egusphere-2025-5159
Preprint. Discussion started: 3 December 2025

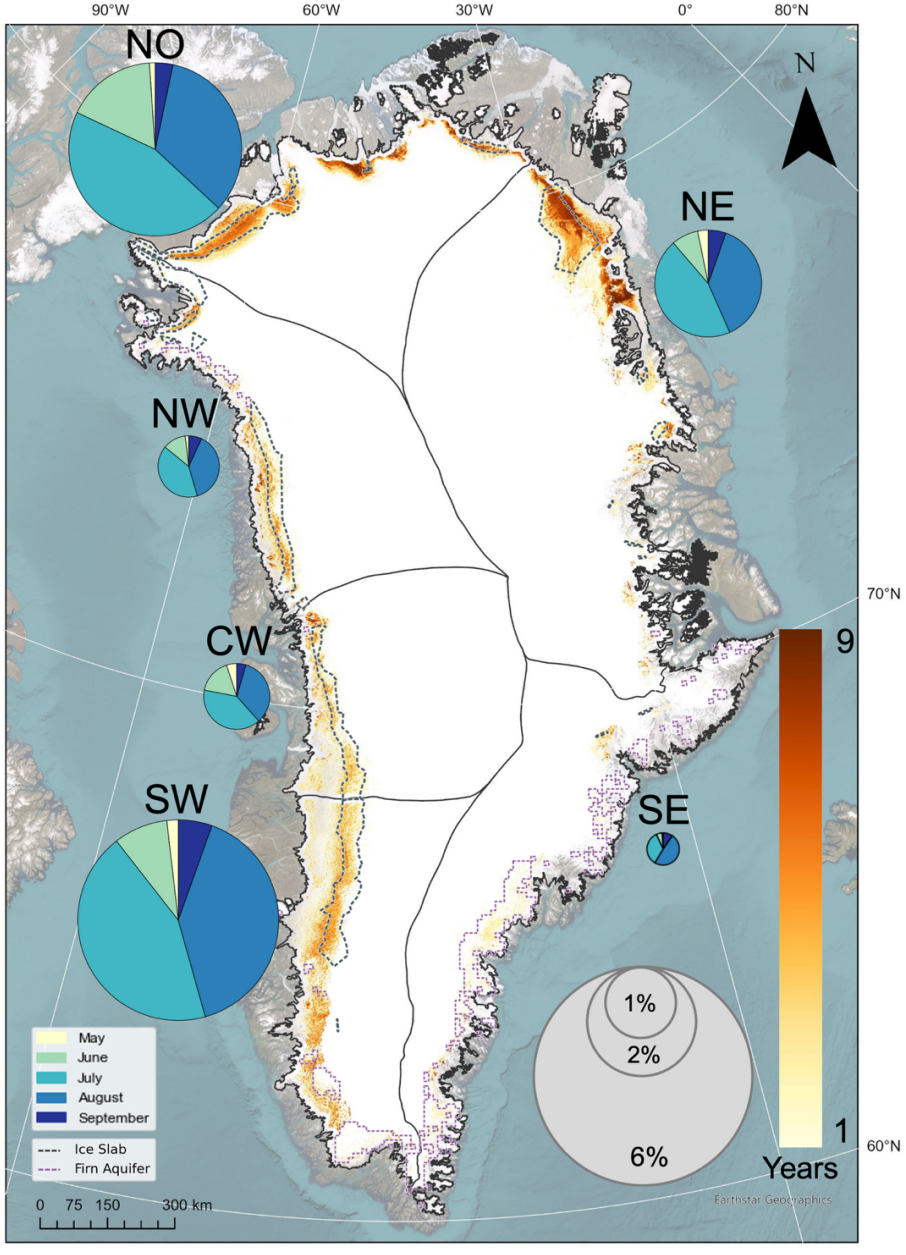

Figure 3. Slush persistence (years) and mean areal extent (% basin area) across GrIS basins during summers (1 May to 30 September) from 2016-2024. Slush persistence is represented by the colour bar on a scale from 1 year (light yellow) to 9 years (dark orange). The mean slush areal extent for each basin as a percentage of the total basin area, from 2016-2024, is illustrated by the area of the circles. Within each circle, pie charts display the mean monthly distribution of slush areal extent averaged over all melt seasons. Dark grey dashed outlines depict ice slab extents from 2010–2018 (Jullien et al., 2023), and purple dashed outlines depict firn aquifer extents from 2010–2014 (Miège et al., 2016). Base map source: Esri.

https://doi.org/10.5194/egusphere-2025-5159
Preprint. Discussion started: 3 December 2025

3.2. Ice-sheet-wide inter- and intra-annual variability in slush areal extent and elevation

The areal extent of slush varied considerably from year to year across the GrIS, closely reflecting interannual variability in surface melt derived from RACMO (Noël et al., 2019) (Fig. 4). Across the ice sheet, maximum seasonal slush extent was strongly correlated with mean May–September surface melt ($R^2 = 0.91$, $p < 0.001$; Fig. S4a), whereas the relationship with mean air temperature was weaker ($R^2 = 0.42$), and only significant at $p < 0.1$ (Fig. S4b).

The maximum seasonal areal extent (i.e., the composite slush area from May–September) was lowest in 2018, the weakest melt season of the study period (Fig. 4c), when slush covered just 20,500 km² (~1.2% of the ice sheet; Fig. 4a–b) and RACMO melt anomalies were ~15 mm w.e. below the 1958–2015 mean. The largest extent occurred in 2019, the strongest melt year (Fig. 4c), when slush covered 90,300 km² (~5.2% of the ice sheet) and melt anomalies reached ~40 mm w.e. above mean (Fig. 4c). No statistically significant trend in the maximum seasonal areal extent of slush over the whole ice sheet was observed over the study period.

Superimposed on these interannual variations in slush areal extent from 2016-2024 was a consistent seasonal pattern, with lowest slush areal extents in May and September (typically < 0.2% of the ice sheet area over the 9 years) and peaks in July (1.7%) and August (1.6%) (Fig. 3). This broad seasonal cycle of low early- and late-season areal extent and mid-summer maxima was a defining feature throughout the study period, and consistent with RACMO-derived surface melt and air temperature anomalies, relative to the 1958–2015 climatological mean (Fig. 4b and c). The seasonal cycle was most pronounced in the highest melt year, 2019, when slush reached its greatest July (54,200 km²) and August (67,200 km²) areal extents (Fig. 4b). However, a notable departure from this cycle occurred in September 2022, when slush areal extent (16,000 km²) surpassed that of August by 4,700 km² (Fig. 4b), consistent with a +3°C September air temperature anomaly relative to 1958–2015 mean (Fig. 4d).

Seasonal variability was also evident in the maximum elevation reached by slush each melt season. It fluctuated markedly between years (Fig. 5a), ranging from below 1,300 m a.s.l. in the lowest melt year (2018) to above 1,800 m a.s.l. in the highest melt year (2019). We do not find a statistically significant trend in the maximum slush elevation from 2016 - 2024 at the ice-sheet scale, although we do find a significant positive relationship between maximum slush elevation and maximum slush areal extent across the ice sheet ($p < 0.05$).

https://doi.org/10.5194/egusphere-2025-5159
Preprint. Discussion started: 3 December 2025

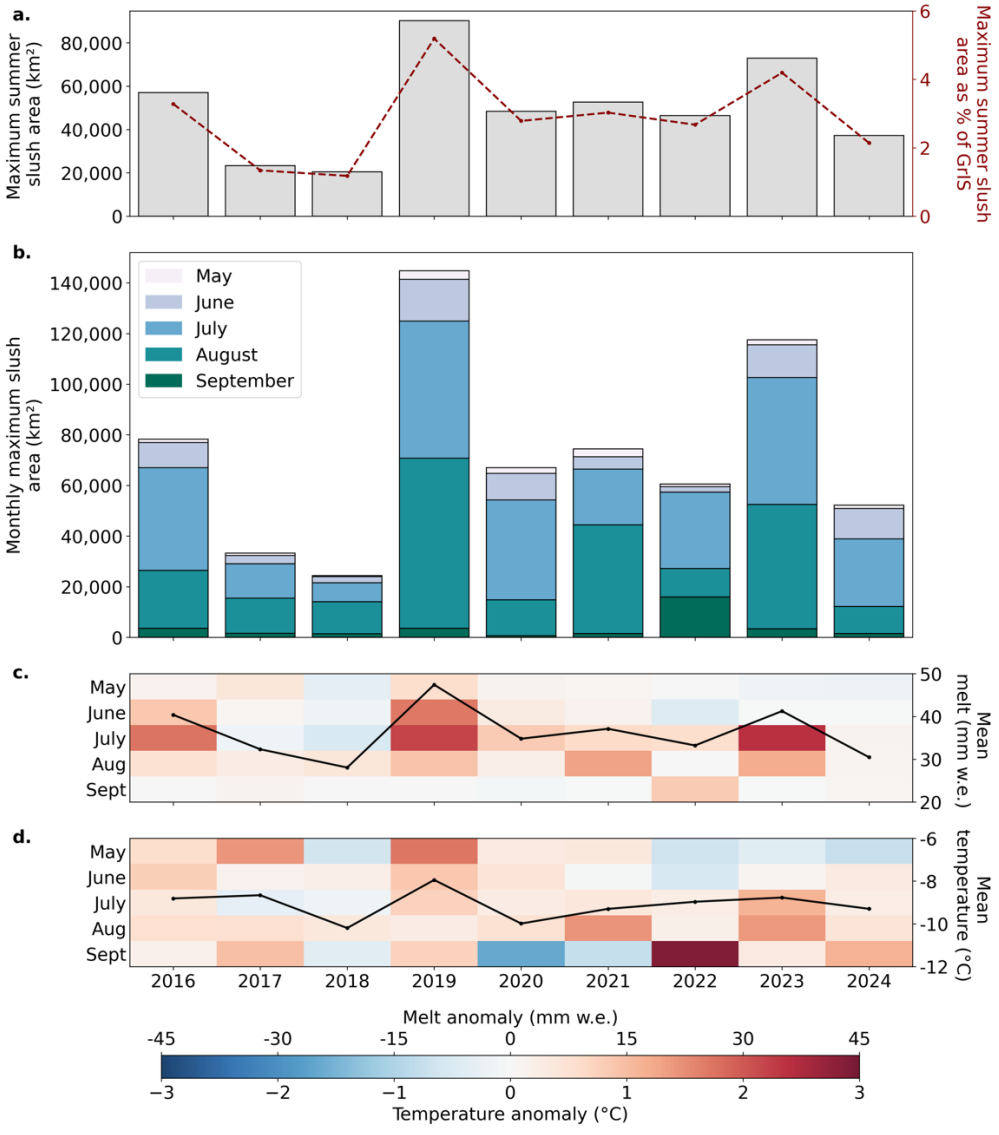

Figure 4. Maximum slush area across the GrIS from 2016–2024. a) Maximum summer slush areal extent from May–September (left y-axis) and as a percentage of ice sheet area (right y-axis; dashed red line). b) Monthly maximum slush area, stacked (May–September) for each year c) Melt anomalies relative to the 1958–2015 monthly mean for each summer month and year from 2016-2024, with mean seasonal melt indicated by the black line (right y-axis). d) Near-surface air-temperature anomalies relative to the 1958–2015 monthly mean for each summer month and year from 2016-2024, with mean summer air temperature indicated by the black line (right y-axis). Melt and air temperature data are derived from RACMO.

https://doi.org/10.5194/egusphere-2025-5159
Preprint. Discussion started: 3 December 2025

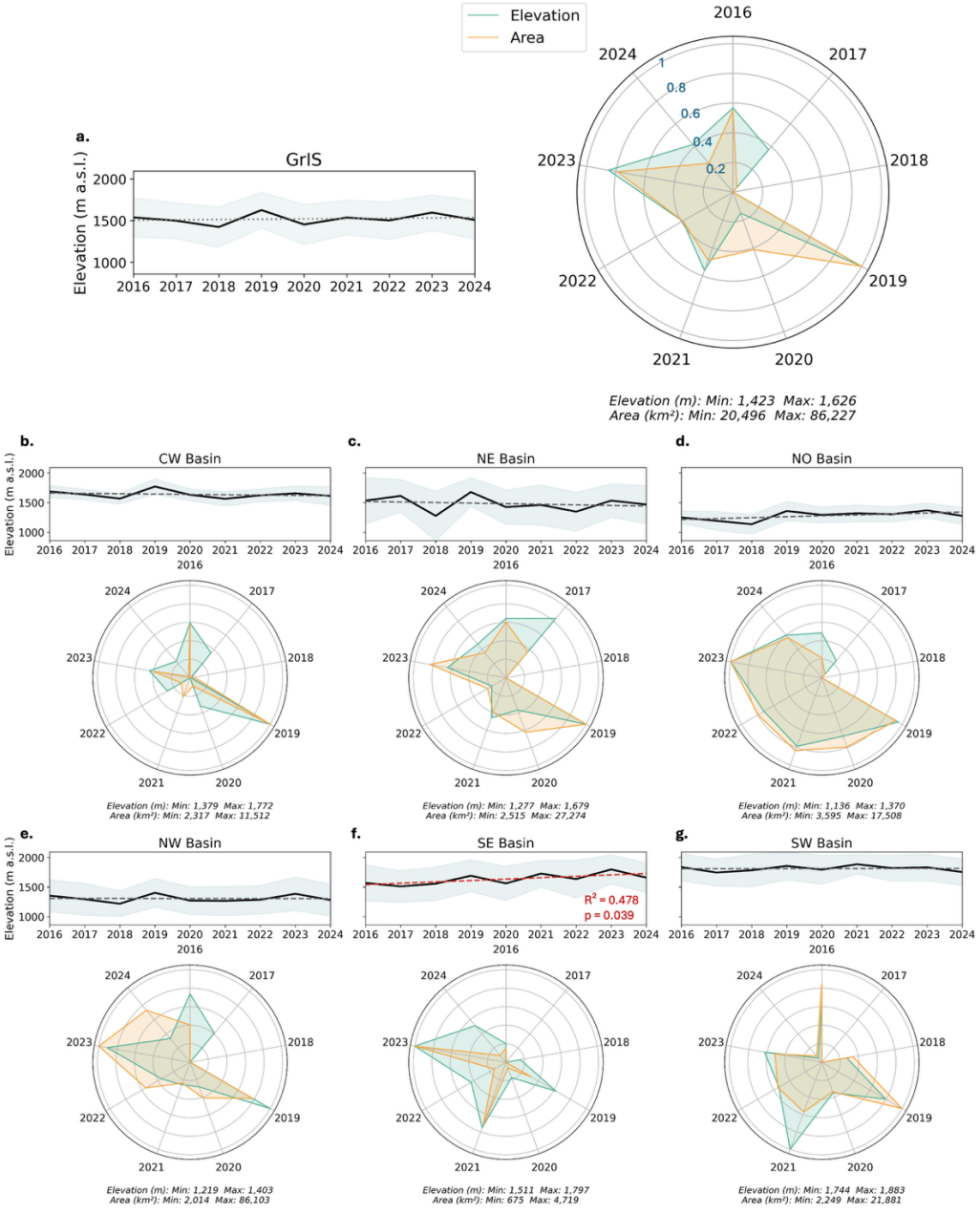

Figure 5. Interannual variability in slush elevation and area from 2016-2024. Panel (a) shows ice-sheet-wide results, while panels (b–g) depict regional results for the six basins (CW, NE, NO, NW, SE, SW). Within each subplot, the line graph shows mean maximum slush elevation (m a.s.l.) from 2016-2024 with ± 1 standard deviation shading and a fitted linear trend line (dotted: red if statistically significant at $p < 0.05$, grey if not). The radar chart in each subplot shows the mean annual maximum slush elevation and area from 2016–2024, with both variables normalised through scaling from 0 to 1, representing the minimum and maximum observed values, respectively.

https://doi.org/10.5194/egusphere-2025-5159
Preprint. Discussion started: 3 December 2025

3.3. Regional inter- and intra-annual variability in slush areal extent and elevation

At the regional scale, interannual variability in slush areal extent broadly echoed the ice-sheet-wide pattern over the nine-year period (Section 3.2), though the magnitude and precise timing of changes differed by region (Fig. 6). In the highest melt year of 2019, all drainage basins experienced peak or near-peak slush areal extent: the SW reached a maximum seasonal areal extent of 22,530 km² (i.e., 10.7% of the basin area), the NE 27,280 km² (5.6%), the NO 16,460 km² (6.8%), the CW 11,520 km² (4.9%) and the NW 10,490 km² (3.8%). Other high-melt years also saw elevated slush areal extent in specific regions. For instance, in 2023, the second greatest melt season in the time series, both the NO and SE basins recorded their maximum slush areas of the time series (17,520 km², i.e., 7.2% of the basin in the NO and 4,890 km² and 1.7%) in the SE). Post-2019, the NO basin notably maintains a consistently higher slush area than pre-2019 levels, a pattern not observed in any other region.

Regional intra-annual variations in slush areal extent over the nine-year period also demonstrated variations in the timing and magnitude of peak slush area (Fig. 6). August 2019 marked the greatest monthly slush areal extent during the time series for all basins except the SE (Fig. 6): the SW basin contained 17,950 km² of slush in August 2019 (8.5% of its area), the NE reached ~20,460 km² (4.2%), the NO ~12,450 km² (5.1%), the NW ~8,130 km² (2.9%), and the CW ~7,140 km² (3.1%). September 2022 saw an atypical late-season resurgence in slush areal extent that was above the time series average across most basins (Fig. 6). Notably, September 2022 was the month of peak slush area for the SW basin (Fig. 6f); the only instance in the record where the annual maximum occurred in September rather than July or August. The preceding month, August 2022, recorded substantially lower values across all basins (e.g. SW: ~1,780 km², 0.8%; NE: ~2,830 km², 0.6%), highlighting the atypical nature of this late-season peak.

Across the six drainage basins, slush areal extent exhibited positive correlations with RACMO-derived mean May–September melt (mm w.e.), with R^2 values ranging from 0.46 (SE) to 0.95 (CW), which were all significant at $p \leq 0.05$ (Fig. S5). In contrast, the relationship between slush extent and mean May–September 2 m air temperature (°C) was not significant in any basin (Fig. S6). These results likely reflect how air temperature is not the sole driver of meltwater (and hence slush) production, and that other components of the surface energy balance play a dominant role.

The maximum elevation reached by slush varied markedly between basins and years (Fig. 5). Such elevations were generally higher in the highest melt years of 2019 (e.g., CW: 1,770 m a.s.l, NE: 1,700 m a.s.l, NO: 1,370 m a.s.l) and 2023 (e.g. SE: 1,800 m a.s.l, NW: 1,470 m a.s.l), and lower in the lower melt years of 2018 and 2020 (e.g. NE: 1,290 m a.s.l in 2018; CW: 1,380 m a.s.l in 2020). Some basins showed distinct inter-annual changes in maximum slush elevation; for example, in the NE basin, an increase of > 400 m occurred between 2018 and 2019. Notably, peak slush elevation did not always coincide with years of peak slush areal extent; for instance, the SW reached its highest elevation in 2021 (1880 m a.s.l), two years after its areal maximum in 2019 (Fig. 5g). A weak statistically significant increasing trend in maximum slush elevation was observed

https://doi.org/10.5194/egusphere-2025-5159
Preprint. Discussion started: 3 December 2025

in the SE basin from 2016 to 2024, with a mean increase of 23.5 m/year ($p < 0.05$, $R^2 = 0.48$; Fig. 5f). No other basins exhibited statistically significant trends between these two variables during the study period.

We found a significant positive relationship between maximum slush elevation and maximum slush areal extent across all basins ($p < 0.05$; Fig. 7). The strength of this relationship varied regionally, with the strongest correlations in the NO ($R^2 = 0.91$) and SE ($R^2 = 0.81$) basins, moderate correlations in SW ($R^2 = 0.70$) and CW ($R^2 = 0.74$), and weaker correlations in NE ($R^2 = 0.60$) and NW ($R^2 = 0.49$). We also found that northern basins (NO, NE, NW) generally sustained higher slush elevations for a given areal extent compared to southern basins (SW, SE, CW).

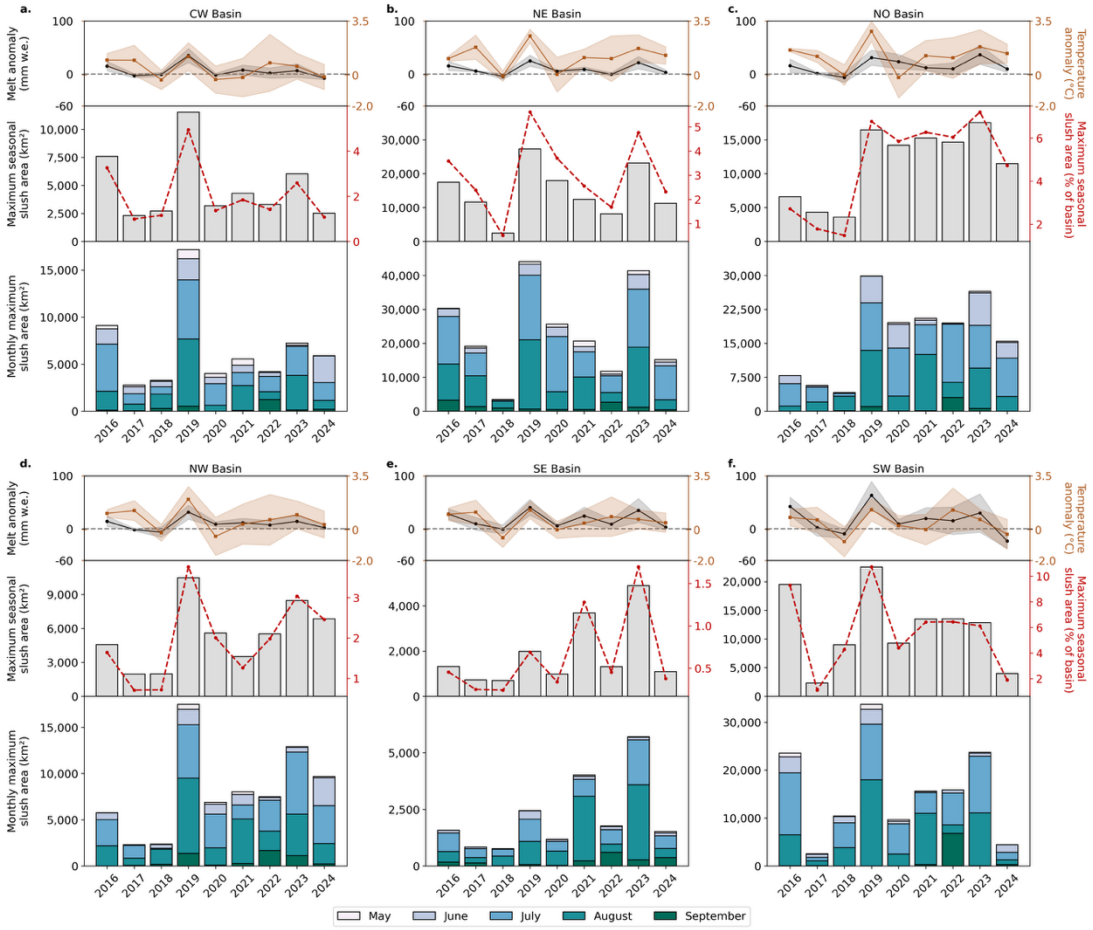

Figure 6. Plots illustrating the total slush area alongside melt and air temperature anomalies from 2016-2024 for the six basins of the GrIS (subplots a - f). Within each subplot, the upper panel displays RACMO-derived melt (black) and air temperature anomalies (red), both averaged over the May–September period. Shaded regions indicate ± 1 standard error of the monthly means. The middle panel shows maximum seasonal slush areal extent from May–September, with the right y-axis showing this as a percentage of the basin area. The bottom panel shows the total slush area (km²), segmented by month (May, June, July, August, and September) for each melt season.

https://doi.org/10.5194/egusphere-2025-5159
Preprint. Discussion started: 3 December 2025

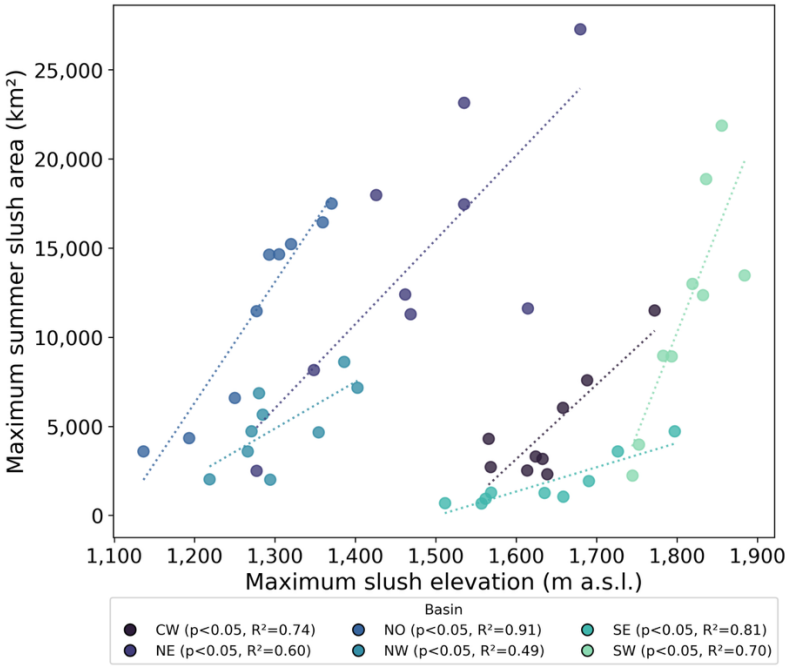

330 **Figure 7. Relationship between maximum elevation and maximum areal extent of slush by basin (2016–2024). Coloured points show annual values, with dotted lines indicating least-squares regressions. All relationships are significant ($p < 0.05$).**

4. Discussion

To the best of our knowledge, our work forms the first large-scale assessment of slush on the GrIS. Existing assessments have
335 almost exclusively focused on well-defined supraglacial meltwater features, specifically, lakes, streams, and water-filled crevasses (e.g., Zhang et al. 2023, Fan et al., 2025; Dunmire et al., 2021; 2025) that are somewhat easier to map using traditional thresholding methods. By leveraging ML within a cloud-based framework, we show that slush can be systematically mapped across the entire ice sheet at high spatial resolution. The resulting nine-year, ice-sheet-wide dataset offers new insight into the spatial variability and persistence of slush, revealing that slush is a widespread and climatically sensitive component of the
340 surface hydrological system feature on the GrIS.

4.1. Slush dominates the areal extent of surface meltwater on the GrIS

Between 2016 and 2024, we show that slush covered a mean area of 2.9% (50,400 km²) of the GrIS each summer, with a peak areal extent of 5.2 % (90,300 km²) in 2019, the year of highest melt in our study period (Figs. 3 and 4). In the same year, Zhang

https://doi.org/10.5194/egusphere-2025-5159
Preprint. Discussion started: 3 December 2025

et al. (2023) mapped a maximum area of 9,990 km² for lakes, streams, and water-filled crevasses; slush therefore covered over nine times more of the GrIS than these other meltwater features in 2019. Even in the lowest melt year of our study period, 2018, our mapped slush areal extent (1.2%; 20,500 km²) was over four times greater than the 4,900 km² of other meltwater features reported by Zhang et al (2023) for 2018. Studies focusing solely on supraglacial lakes highlight an even greater disparity. Fan et al. (2025) showed that between 1985 and 2023, supraglacial lake area rarely exceeded 3,500 km², with a total of ~3,000 km² in 2019. Similarly, Dunmire et al. (2021) reported total supraglacial lake areas of 1,242 km² in 2018 and 2,569 km² in 2019. In both cases, total areas of slush observed in our study exceeded total lake areal extents by ~16 times in 2018 and ~35 times in 2019.

At the basin scale, our slush areal extent observations also greatly surpass the areal extent of other meltwater features observed previously. For example, for the NE in 2019, we detected a maximum slush areal extent of 27,280 km², whereas Zhang et al. (2023) reported just 820 km² of other meltwater features in this basin; a more than 30-fold difference.

Although the aforementioned cross-study comparisons reflect differing methodologies; we use them to illustrate relative scale. These comparisons demonstrate that slush is the most extensive surface meltwater feature on the GrIS, especially since our slush areas likely represent lower bounds, as optical sensors capture only surface slush and cannot detect subsurface saturation. The true difference in areal extents between slush and other meltwater features may therefore be even larger than estimated here.

4.2. Slush is most extensive in the Western and Northern basins

Our observations reveal that slush is most extensive in the western (notably the SW) and northern basins of the GrIS, and least extensive in the eastern and southeastern basins. This distribution aligns with observations from previous supraglacial hydrology studies, which report more extensive meltwater features in west Greenland, particularly supraglacial lakes (e.g., Selmes et al., 2011; Hu et al., 2022; Zhang et al., 2023; Fan et al., 2025; Dunmire et al., 2021; 2025).

In the SW basin, low-angle slopes, broad ablation zones (Ryan et al., 2019), and high melt rates (Mikkelsen et al., 2016; van As, 2017) create conditions that likely allow slush to extend further inland than in other regions. A disproportionate loss of firn air content relative to other regions (Vandecrux et al., 2019) may also promote widespread surface saturation and slush formation in the SW. Although these conditions favour extensive inland slush in much of the SW basin, the western margin coincides with the “dark zone” (Tedstone et al., 2017), where limited snow cover may restrict slush formation, producing a distinct stripe of low slush persistence parallel with the western margin (Fig. 3).

The dominance of slush we observed in the western and northern regions of the ice sheet may also be linked to the prevalence of pre-existing low-permeability ice slabs. Ice slabs inhibit vertical meltwater percolation and promote sustained saturation of the firn above, leading to slush formation that encourages lateral meltwater transport and runoff (Machguth et al., 2016;

https://doi.org/10.5194/egusphere-2025-5159
Preprint. Discussion started: 3 December 2025

MacFerrin et al., 2019; Jullien et al., 2023). We calculate that about 30% (45,100 km²) of Greenland's slush area lies above ice slabs, with most of this concentrated in the western and northern basins (Fig. 3). An additional ~10% (8,330 km²) of slush forms above firn aquifers (i.e., saturated subsurface reservoirs), which are mainly present in the SE basin and may contribute to slush formation via their rising water table during intense melt events (Forster et al., 2014; Miege et al., 2016). The remaining 60% of slush areal extent occurs in regions lacking underlying low-permeability layers (Fig. 3), instead forming when when the rate of meltwater production exceeds the firn's capacity to absorb and facilitate water percolation. Achieving full firn saturation is more challenging under these conditions, as the firn must become saturated at depth, which typically occurs when preferential flow fingers are overwhelmed and a uniform wetting front saturates the surface layers (Clerx et al., 2022; 2024).

Persistence patterns mirror these distributions (Fig. 3): slush is generally more persistent above ice slabs, reflecting the sustained saturation they promote, whereas slush above firn aquifers appears less persistent, consistent with their more variable hydrological influence.

Together, the spatial and temporal persistence patterns that we observe indicate that while pre-existing low-permeability structures may exert a control on where slush is most stable and recurrent, extensive slush formation does also occur in regions without slabs or aquifers when melt intensity overwhelms firn storage capacity. However, fully resolving the physical coupling between slush occurrence, firn stratigraphy, permeability, and refreezing capacity requires dedicated future work. The dataset presented here provides a new observational foundation for such integrative analyses.

4.3. Slush reaches higher elevations *and* is greater in areal extent during extreme melt years

In extreme melt years (notably 2019 and 2023; the highest and second highest melt seasons in our time series, respectively), slush both reaches higher elevations and is more areally extensive than in cooler, low-melt years (e.g., 2018; Figs. 5 and 6), which also mirrors the established tendency for supraglacial lakes to appear at higher elevations in warmer years (Sundal et al., 2009; Liang et al., 2012; Lüthje et al., 2006; Leeson et al., 2015; Glen et al., 2025). Under typical conditions, we show that variability in the areal extent in slush follows a predictable seasonal cycle, forming in May, peaking in areal extent and maximum elevation in July, and decreasing in area during the autumn freeze-up, similar again to the behaviour of supraglacial lakes (e.g., Otto et al., 2022; Yang et al., 2021; Glen et al., 2025). During extreme high melt years such as 2019, this seasonal cycle is amplified, with sustained high air temperatures combined with melt-albedo feedbacks producing prolonged, intense melt (Sasgen et al., 2020; Tedesco & Fettweis, 2020; Hanna et al., 2021), which likely drove 2019 to have the most extensive and furthest inland slush areal extents in our record. In contrast, we suggest that the atypical pattern in 2022 resulted from a late-season, anonymously warm and rainy event in September 2022 that triggered ice-sheet–wide melt and delayed late-season freeze-up (Moon et al., 2022; C3S, 2023), enabling the sustained slush presence that we observed into October 2022.

Despite the strong interannual variability in slush elevation and area that we observe, our nine-year record reveals no statistically significant trend in slush area or elevation at either ice-sheet or regional scales, except from a weak elevation

https://doi.org/10.5194/egusphere-2025-5159
Preprint. Discussion started: 3 December 2025

increase in the SE basin ($R^2 = 0.478$, $p < 0.05$). These results are consistent with Machguth et al. (2022), who, over a similar length study period (2012–2021), found no significant change in maximum slush elevation on the western GrIS, but observed pronounced intra-seasonal variability. Multi-decadal studies, however, have reported increases in meltwater feature area and elevation over time. For example, Fan et al. (2025) documented an ice-sheet-wide supraglacial lake area increase of ~50.5 km² yr^{-1} from 1985–2023, while Tedstone and Machguth (2022) reported increases in visible runoff limits of ~242 m (west), 194 m (north), and 59 m (northeast) between 1985–2020. These findings suggest that while inter- and intra-annual variability dominate decadal slush records, slush is nonetheless likely to follow the broader trajectory of increasing area and elevation over multi-decadal timescales.

Our observations suggest that extreme melt events not only drive widespread slush formation through direct surface melt, but they may also precondition the ice sheet for slush recurrence in subsequent melt seasons driving greater persistence. For example, the NO basin exhibited elevated slush areal extent in all years after the extreme 2019 melt season (Fig. 6c), even when melting was low. This is suggestive of a 'legacy' effect, where slush that formed during 2019 refroze to produce low-permeability firn and/or thicken pre-existing ice slabs, reducing firn infiltration capacity. In later years, only the seasonal snowpack needs to saturate to regenerate slush. This interpretation is consistent with recent work by Rawlins et al. (2023), who documented earlier melt onset and prolonged melt seasons in northern Greenland following major slush events in previous years.

The sensitivity of slush formation to extreme melt events, as observed in this study, highlights its potential for rapid areal expansion under continued atmospheric warming. Combined with Arctic amplification and ice–climate feedbacks driving longer and more frequent intense melt seasons on the GrIS (Hanna et al., 2024), this suggests that slush may not only expand rapidly during peak melt events but may also persist later into the season due to delayed freeze-up, thereby extending its role as an active component of the hydrological regime. These changes may alter surface and subglacial meltwater routing, impact ice dynamics and mass balance, and ultimately affect the ice sheet's contribution to sea-level rise.

4.4. Implications for surface energy balance and hydrological modelling

Slush plays a key role in regulating glacier surface energy balance and meltwater pathways, and accurately representing its presence and dynamics in energy-balance (e.g. Noel et al., 2019; Huai et al., 2020) and surface hydrological (e.g. Banwell et al., 2012; Leeson et al., 2012) models is essential to capture realistic albedo–melt feedbacks, meltwater storage capacity, and connectivity between supraglacial hydrological features. Incorporating time-varying slush layers can improve estimates of surface albedo reduction (Ryan et al., 2025) and melt (Dell et al., 2024), while accounting for its temporary storage and connectivity functions may improve predictions of surface and subglacial water routing, ice dynamics, and the ice sheet's seasonal evolution (e.g., de Fleurian et al., 2018). Observations such as those presented here provide a well-constrained input to refine these hydrological models and better capture the complex interactions between meltwater and ice-sheet processes.

https://doi.org/10.5194/egusphere-2025-5159
Preprint. Discussion started: 3 December 2025

5. Conclusion

We present the first high spatial resolution, ice-sheet-wide record of slush on the GrIS, spanning nine melt seasons (2016–2024). Using > 300,000 S2 images and a supervised RF workflow in GEE, we show that slush is widespread, climate-sensitive, and the dominant surface meltwater feature on the GrIS: it covers a mean ~2.9% of the ice sheet each summer and in the high melt year of 2019, it covered an area nine times greater than the total area of other meltwater features (supraglacial lakes, rivers, and water filled crevasses) reported in other studies. Slush expands inland to higher elevations in warmer years and is widely concentrated over low-permeability ice slabs in the northern and western basins. Explicit representation of slush in surface mass-balance, routing, and coupled hydrology–ice dynamics models is therefore necessary to capture Greenland's evolving surface hydrology and runoff. As melt seasons lengthen and intensify, slush will likely become even more widespread. Continued development of high-resolution, multi-feature supraglacial meltwater datasets, which explicitly partition slush, will play a key role in understanding Greenland's future evolution.

Data availability

The slush dataset produced in this study is available from: https://doi.org/10.5281/zenodo.16338735 (Glen, 2025). The slush delineation code used in this study is available from https://doi.org/10.17863/CAM.77156). Sentinel 2 imagery is freely available via the GEE data catalogue (https://developers.google.com/earth-engine/datasets/catalog/sentinel). RACMO2.3p2 model data are available upon request from B. Noël (bnoel@uliege.be).

Author contributions

EG, AFB and AL conceptualised the research, which was led by EG. AFB, AL, KM, RD, JM and MM contributed to the scientific content, technical details and overall structure of this paper. All co-authors contributed to the discussion of results and editing of the manuscript.

Competing interests

The authors have no competing interests to declare.

Acknowledgements

Emily Glen and Amber Leeson received support from the Natural Environment Research Council (NERC) MIIGreenland project under award NE/S011390/1 and from the European Space Agency under the POLAR+ 4DGreenland project, ESA contract no. 4000132139/20/I-EF. Alison F. Banwell received support from the U.S. National Science Foundation (NSF) under awards 1841607 and 2332480 to the University of Colorado Boulder (PI Banwell). Malcolm McMillan was supported by the European Space Agency POLAR+ 4DGreenland project (contract no. 4000132139/20/I-EF) and the Lancaster University–

https://doi.org/10.5194/egusphere-2025-5159
Preprint. Discussion started: 3 December 2025

UKCEH Centre of Excellence in Environmental Data Science. Malcolm McMillan and Jennifer Maddalena were supported by the UK NERC Centre for Polar Observation and Modelling (grant no: NE/Y006178/1).

Financial support

This research has been supported by the Natural Environment Research Council (grant no's. NE/S011390/1 and NE/Y006178/1), the European Space Agency (grant no. 4000132139/20/I-EF), the National Science Foundation (grant no. 1841607 and 2332480).

References

Banwell, A. F., Hewitt, I., Willis, I. C., and Arnold, N.: Moulin density controls drainage development beneath the Greenland ice sheet, J. Geophys. Res. Earth Surf., 121, 2248–2269, https://doi. org/10. 1002/2015JF003801, 2016.

Banwell, A. F., I. C. Willis, I. C., and Arnold N. S.: Modeling subglacial water routing at Paakitsoq, W Greenland, J. Geophys. Res. Earth Surf., 118, 1282–1295, https://doi. org/10. 1002/jgrf. 20093, 2013.

Banwell, A. F., Wever, N., Dunmire, D., and Picard, G.: Quantifying Antarctic-wide ice-shelf surface melt volume using microwave and firn model data: 1980 to 2021, Geophysical Research Letters, 50, e2023GL102744, https://doi.org/10.1029/2023GL102744, 2023.

Banwell, A. F., Arnold, N. S., Willis, I. C., Tedesco, M., and Ahlstrøm, A. P.: Modeling supraglacial water routing and lake filling on the Greenland Ice Sheet, J. Geophys. Res., 117, F04012, https://doi. org/10. 1029/2012JF002393, 2012.

Bonsoms, J., Oliva, M., López-Moreno, J. I., and Fettweis, X.: Rising extreme meltwater trends in Greenland Ice Sheet (1950–2022): Surface energy balance and large-scale circulation changes. J. Clim., 37, 4851–4866, https://doi.org/10.1175/JCLI-D-23-0396.1, 2024.

Box, J. E. and Ski, K.: Remote sounding of Greenland supra-glacial melt lakes: Implications for subglacial hydraulics, Journal of glaciology, 53(181), 257−264, https://doi. org/10. 3189/172756507782202883, 2007.

Breiman, L.: Random forests, Mach. Learn., 45, 5–32, https://doi.org/10.1023/A:1010933404324, 2001.

Chu, V. W.: Greenland ice sheet hydrology: A review, Prog. Phys. Geogr., 38, 19–54, https://doi.org/10.1177/0309133313507075, 2014.

Chudley, T. R., Christoffersen, P., Doyle, S. H., Dowling, T. P. F., Law, R., Schoonman, C. M., Bougamont, M., and Hubbard, B.: Controls on water storage and drainage in crevasses on the Greenland Ice Sheet, J. Geophys. Res. Earth Surf., 126, e2021JF006287, https://doi.org/10.1029/2021JF006287, 2021.

Clerx, N., Machguth, H., Tedstone, A., and van As, D.: Modelling lateral meltwater flow and superimposed ice formation atop Greenland's near-surface ice slabs. J. Glaciol., 70, e54, https://doi.org/10.1017/jog.2024.69, 2024.

https://doi.org/10.5194/egusphere-2025-5159
Preprint. Discussion started: 3 December 2025

Clerx, N., Machguth, H., Tedstone, A., Jullien, N., Wever, N., Weingartner, R., and Roessler, O.: 'In situ measurements of meltwater flow through snow and firn in the accumulation zone of the SW Greenland ice sheet', The Cryosphere, 16, 4379–4401. https://doi.org/10.5194/tc-16-4379-2022, 2022.

Cogley, J. G., Arendt, A. A., Bauder, A., Braithwaite, R. J., Hock, R., Jansson, P., Kaser, G., Möller, M., Nicholson, L., Rasmussen, L. A., & Zemp, M. (2010). Glossary of glacier mass balance and related terms. IHP-VII Technical Documents in Hydrology, 86, International Hydrological Programme, UNESCO, Paris, France.

Copernicus Climate Change Service (C3S): European State of the Climate 2022, Summary, https://climate.copernicus.eu/sites/default/files/custom-uploads/ESOTC2022/PR/ESOTCsummary2022_final.pdf, last access: December 2024.

Corr, D., Leeson, A., McMillan, M., Zhang, C., and Barnes, T.: An inventory of supraglacial lakes and channels across the West Antarctic Ice Sheet, Earth Syst. Sci. Data, 14, 209–228, https://doi. org/10. 5194/essd-14-209-2022, 2022.

Covi, F.: Processes in the percolation zone in southwest Greenland: challenges in modeling surface energy balance and melt, and the role of topography in the formation of ice slabs. PhD dissertation, University of Alaska Fairbanks, 2022. Available at: https://hdl.handle.net/11122/13116, 2022.

Culberg, R., Michaelides, R. J., & Miller, J. Z. (2024). Sentinel-1 detection of ice slabs on the Greenland ice sheet. The Cryosphere, 18(5), 2531–2555. https://doi.org/10.5194/tc-18-2531-2024

de Fleurian, B., Werder, M. A., Beyer, S., Brinkerhoff, D. J., Delaney, I., Dow, C. F., SHMIP the subglacial hydrology model intercomparison project. Journal of Glaciology, 64(248), 897–916. https://doi.org/10.1017/jog.2018.78, 2018

Dell, R. L., Banwell, A. F., Willis, I. C., Arnold, N. S., Halberstadt, A. R. W., Chudley, T. R., and Pritchard, H. D.: Supervised classification of slush and ponded water on Antarctic ice shelves using Landsat 8 imagery, Journal of Glaciology, 68, 401–414, 2022.

Dell, R.L., Willis, I.C., Arnold, N.S., Banwell, A., de Roda Husman, S.: Substantial contribution of slush to meltwater area across Antarctic ice shelves. Nat. Geosci. 17, 624–630, https://doi.org/10.1038/s41561-024-01466-6, 2024.

Dirscherl, M., Dietz, A. J., Kneisel, C., and Kuenzer, C.: Automated Mapping of Antarctic Supraglacial Lakes Using a Machine Learning Approach. Remote Sens., 12, 1203, https://doi.org/10.3390/rs12071203, 2020.

Dunmire, D., Banwell, A. F., Wever, N., Lenaerts, J. T. M., and Datta, R. T.: Contrasting regional variability of buried meltwater extent over 2 years across the Greenland Ice Sheet, The Cryosphere, 15, 2983–3005, https://doi.org/10. 5194/tc-15-2983-2021, 2021.

Dunmire, D., Subramanian, A. C., Hossain, E., Gani, M. O., Banwell, A. F., Younas, H., and Myers, B.: Greenland Ice Sheet wide supraglacial lake evolution and dynamics: Insights from the 2018 and 2019 melt seasons, Earth and Space Science, 12, e2024EA003793, https://doi.org/10.1029/2024EA003793, 2025.

Fan, Y., Ke, C.-Q., Luo, L., Shen, X., Livingstone, S. J., and Lea, J. M.: Expansion of supraglacial lake area, volume, and extent on the Greenland Ice Sheet from 1985 to 2023, Journal of Glaciology, 71, e4, https://doi.org/10.1017/jog.2024.87, 2025.

https://doi.org/10.5194/egusphere-2025-5159
Preprint. Discussion started: 3 December 2025

Fettweis, X., Tedesco, M., van den Broeke, M. and Ettema, J.: Melting trends over the Greenland ice sheet (1958-2009) from spaceborne microwave data and regional climate Models, The Cryosphere, 5(2), 359-375, ISSN 19940416, doi: 10.5194/tc-5-359-2011, 2011.

Forster, R. R., Box, J. E., van den Broeke, M. R., Miège, C., Burgess, E. W., van Angelen, J. H., Lenaerts, J. T. M., Koenig, L. S., Paden, J., Lewis, C., Gogineni, S. P., Leuschen, C., and McConnell, J. R.: Extensive liquid meltwater storage in firn within the Greenland ice sheet. Nat. Geosci., 7, 95–98, https://doi.org/10.1038/ngeo2043, 2014.

Glen, E., Leeson, A., Banwell, A. F., Maddalena, J., Corr, D., Atkins, O., Noël, B., and McMillan, M.: A comparison of supraglacial meltwater features throughout contrasting melt seasons: southwest Greenland, The Cryosphere, 19, 1047–1066, https://doi.org/10.5194/tc-19-1047-2025, 2025.

Greuell, W. and Knap, W. H.: 'Remote sensing of the albedo and detection of the slush line on the Greenland ice sheet', J. Geophys. Res.-Atmos., 105, 15567–15576, https://doi.org/10.1029, 2000.Halberstadt, A.R.W., Gleason, C.J., Moussavi, M.S., Pope, A., Trusel, L.D., DeConto, R.M. Antarctic Supraglacial Lake Identification Using Landsat-8 Image Classification, Remote Sens, 12, 1327, https://doi.org/10.3390/rs12081327, 2020

Halberstadt, A. R. W., Gleason, C. J., Moussavi, M. S., Pope, A., Trusel, L. D., and DeConto, R. M.: Antarctic Supraglacial Lake Identification Using Landsat-8 Image Classification. Remote Sens., 12, 1327, https://doi.org/10.3390/rs12081327, 2020.

Hanna E, Cappelen J, Fettweis X, Mernild, S. H., Mote, T. L., Mottram, R., Steffen, K., Ballinger, and T. J., Hall, R. J: Greenland surface air temperature changes from 1981 to 2019 and implications for ice-sheet melt and mass-balance change. Int J Climatol. 2021;41 (Suppl. 1), E1336–E1352, https://doi.org/10.1002/joc.6771, 2021.

Hanna, E., Topál, D., Box, J. E., Buzzard, S., Christie, F. D. W., Hvidberg, C., Morlighem, M., De Santis, L., Silvano, A., Colleoni, F., Sasgen, I., Banwell, A. F., van den Broeke, M. R., DeConto, R., De Rydt, J., Goelzer, H., Gossart, A., Gudmundsson, G. H., Lindbäck, K., Miles, B., Mottram, R., Pattyn, F., Reese, R., Rignot, E., Srivastava, A., Sun, S., Toller, J., Tuckett, P. A., and Ultee, L.: Short- and long-term variability of the Antarctic and Greenland ice sheets, Nat. Rev. Earth Environ., 5, 193–210, https://doi.org/10.1038/s43017-024-00438-8, 2024.

Hofer, S., Tedstone, A. J., Fettweis, X., and Bamber, J. L.: Decreasing cloud cover drives the recent mass loss on the Greenland Ice Sheet, Science Advances, 3, e1700584, https://doi.org/10.1126/sciadv.1700584, 2017.

Holmes, C. W.: 'Morphology and Hydrology of the Mint Julep Area, Southwest Greenland. In: Project Mint Julep Investigation of Smooth Ice Areas of the Greenland Ice Cap, 1953; Part II Special Scientific Reports.', Arctic, Desert, Tropic Information Center; Research Studies Institute; Air University, 1955.

Howat, I. M., de la Peña, S., van Angelen, J. H., Lenaerts, J. T. M., and van den Broeke, M. R.: Brief Communication "Expansion of meltwater lakes on the Greenland Ice Sheet", The Cryosphere, 7, 201–204, https://doi. org/10. 5194/tc-7-201-2013, 2013.

Hu, J., Huang, H., Chi, Z., Cheng, X., Wei, Z., Chen, P., Xu, X., Qi, S., Xu, Y., and Zheng, Y.: Distribution and evolution of supraglacial lakes in Greenland during the 2016–2018 melt seasons, Remote Sensing, 14, 55, 2021.

https://doi.org/10.5194/egusphere-2025-5159
Preprint. Discussion started: 3 December 2025

Huai, B., van den Broeke, M. R., and Reijmer, C. H.: Long-term surface energy balance of the western Greenland Ice Sheet and the role of large-scale circulation variability, The Cryosphere, 14, 4181–4199, https://doi.org/10.5194/tc-14-4181-2020, 2020.

IMBIE.: Mass balance of the Greenland Ice Sheet from 1992 to 2018, Nature, 579, 233-239, https://doi.org/10.1038/s41586-019-1855-2, 2020.

Jullien, N., Tedstone, A. J., Machguth, H., Karlsson, N. B., and Helm, V.: Greenland Ice Sheet ice slab expansion and thickening, Geophys. Res. Lett., 50, e2022GL100911, https://doi.org/10.1029/2022GL100911, 2023.

Koziol CP and Arnold N: Modelling seasonal meltwater forcing of the velocity of land-terminating margins of the Greenland Ice Sheet. Cryosphere, 12(3), 971–991, 2018

Leeson, A. A., Shepherd, A., Briggs, K., Howat, I., Fettweis, X., Morlighem, M., and Rignot, E.: Supraglacial lakes on the Greenland ice sheet advance inland under warming climate, Nat Clim Chang, 5, 51–55. https://doi. org/10.1038/nclimate2463, 2015.

Leeson, A. A., Shepherd, A., Palmer, S., Sundal, A., and Fettweis, X.: Simulating the growth of supraglacial lakes at the western margin of the Greenland ice sheet, The Cryosphere, 6, 1077–1086, https://doi. org/10. 5194/tc-6-1077-2012, 2012.

Liang, Y.-L., Colgan, W., Lv, Q., Steffen, K., Abdalati, W., Stroeve, J., Gallaher, D., and Bayou, N.: A decadal investigation of supraglacial lakes in West Greenland using a fully automatic detection and tracking algorithm, Remote Sensing of Environment, 123, 127–138, https://doi.org/10.1016/j.rse.2012.03.020, 2012.

Lüthje, M., Pedersen, L. T., Reeh, N., and Greuell, W.: Modelling the evolution of supraglacial lakes on the West Greenland ice-sheet margin, J. Glaciol., 52, 608–618, https://doi.org/10. 3189/172756506781828386, 2006.

Machguth, H., MacFerrin, M., van As, D., Box, J. E., Charalampidis, C., Colgan, W., Fausto, R, S., Meijer, H. A. J., Mosley-Thompson., and van de Wal, R. S. W.: Greenland meltwater storage in firn limited by near-surface ice formation. Nature Clim Change 6, 390–393, https://doi. org/10. 1038/nclimate2899, 2016.

Machguth, H., Tedstone, A., and Mattea, E.: Daily variations in Western Greenland slush limits, 2000–2021, Journal of Glaciology, 69(273), 191-203, https://doi.org/10.1017/jog.2022.65, 2023.

McFeeters, S. K.: The use of the Normalized Difference Water Index (NDWI) in the delineation of open water features', International Journal of Remote Sensing, 17(7), 1425–1432, https://doi.org/10.1080/01431169608948714., 1996.

Miège, C., Forster, R. R., Brucker, L., Koenig, L. S., Solomon, D. K., Paden, J. D., Box, J. E., Burgess, E. W., Miller, J. Z., McNerney, L., and Brautigam, N.: Spatial extent and temporal variability of Greenland firn aquifers detected by ground and airborne radars, J. Geophys. Res. Earth Surf., 121, 2381–2398, https://doi.org/10.1002/2016JF003869, 2016.

Mikkelsen, A. B., Hubbard, A., MacFerrin, M., Box, J. E., Doyle, S. H., Fitzpatrick, A., Hasholt, B., Bailey, H. L., Lindbäck, K., and Pettersson, R.: Extraordinary runoff from the Greenland ice sheet in 2012 amplified by hypsometry and depleted firn retention, The Cryosphere, 10, 1147–1159, https://doi.org/10.5194/tc-10-1147-2016, 2016.

https://doi.org/10.5194/egusphere-2025-5159
Preprint. Discussion started: 3 December 2025

Miles K. E., Willis I. C., Benedek, C. L., Williamson, A. G., and Tedesco, M.: Toward Monitoring Surface and Subsurface Lakes on the Greenland Ice Sheet Using Sentinel-1 SAR and Landsat-8 OLI Imagery, Front. Earth Sci. 5:58, https://doi.org/10.3389/feart.2017.00058, 2017.

Moon, T., Mankoff, K., Fausto, R., Fettweis, X., Loomis, B., Mote, T., et al.: Arctic Report Card 2022: Greenland Ice Sheet, NOAA Technical Report OAR ARC 22-05, https://doi.org/10.25923/c430-hb50, 2022.

Moussavi, M., Pope, A., Halberstadt, A. R. W., Trusel, L. D., Cioffi, L., and Abdalati, W.: Antarctic supraglacial lake detection using Landsat 8 and Sentinel-2 imagery: Towards continental generation of lake volumes. Remote Sens., 12(1), 134, https://doi.org/10.3390/rs12010134, 2020.

Noël, B., van de Berg, W. J., Lhermitte, S., and van den Broeke, M. R.: Rapid ablation zone expansion amplifies North Greenland mass loss. Science Advances, 5(9), 2–11. https://doi.org/10.1126/sciadv.aaw0123, 2019.

Otosaka, I. N., Shepherd, A., Ivins, E. R., Schlegel, N.-J., Amory, C., van den Broeke, M. R., Horwath, M., Joughin, I., King, M. D., Krinner, G., Nowicki, S., Payne, A. J., Rignot, E., Scambos, T., Simon, K. M., Smith, B. E., Sørensen, L. S., Velicogna, I., Whitehouse, P. L., A, G., Agosta, C., Ahlstrøm, A. P., Blazquez, A., Colgan, W., Engdahl, M. E., Fettweis, X., Forsberg, R., Gallée, H., Gardner, A., Gilbert, L., Gourmelen, N., Groh, A., Gunter, B. C., Harig, C., Helm, V., Khan, S. A., Kittel, C., Konrad, H., Langen, P. L., Lecavalier, B. S., Liang, C.-C., Loomis, B. D., McMillan, M., Melini, D., Mernild, S. H., Mottram, R., Mouginot, J., Nilsson, J., Noël, B., Pattle, M. E., Peltier, W. R., Pie, N., Roca, M., Sasgen, I., Save, H. V., Seo, K.-W., Scheuchl, B., Schrama, E. J. O., Schröder, L., Simonsen, S. B., Slater, T., Spada, G., Sutterley, T. C., Vishwakarma, B. D., van Wessem, J. M., Wiese, D., van der Wal, W., and Wouters, B.: Mass balance of the Greenland and Antarctic ice sheets from 1992 to 2020, Earth Syst. Sci. Data, 15, 1597–1616, https://doi.org/10.5194/essd-15-1597-2023, 2023.

Otto J, Holmes, F. A. and Kirchner, N.: Supraglacial lake expansion, intensified lake drainage frequency, and first observation of coupled lake drainage, during 1985–2020 at Ryder Glacier, Northern Greenland, Front. Earth Sci.,10:978137, https://doi.org/10.3389/feart.2022.978137, 2022.

Porter, C., Morin, P., Howat, I., Noh, M.-J., Bates, B., Peterman, K., Keesey, S., Schlenk, M., Gardiner, J., Tomko, K.,Willis, M., Kelleher, C., Cloutier, M., Husby, E., Foga, S.,Nakamura, H., Platson, M., Wethington, M. Jr., Williamson,C., Bauer, G., Enos, J., Arnold, G., Kramer, W., Becker, P.,Doshi, A., D'Souza, C., Cummens, P., Laurier, F., and Bo-jesen, M.: ArcticDEM, v3.0, Harvard Dataverse [data set], https://doi.org/10.7910/DVN/OHHUKH, 2023 [Date Accessed: April 2024].

Qayyum, N., Ghuffar, S., Ahmad, H., Yousaf, A., and Shahid, I.: Glacial Lakes Mapping Using Multi Satellite PlanetScope Imagery and Deep Learning. ISPRS Int. J. Geo-Inf., 9, 560, https://doi.org/10.3390/ijgi9100560, 2020.

Rawlins, L. D., Rippin, D. M., Sole, A. J., Livingstone, S. J., and Yang, K.: Seasonal evolution of the supraglacial drainage network at Humboldt Glacier, North Greenland, between 2016 and 2020, The Cryosphere Discuss., https://doi. org/10. 5194/tc-2023-23, 2023.

Rippin, D. and Rawlins, L.: Supraglacial River Networks, In International Encyclopedia of Geography, edited by: Richardson, D., Castree, N., Goodchild, M. F., Kobayashi, A., Liu, W., and Marston, R. A., https://doi.org/10.1002/9781118786352.wbieg2072, 2021

https://doi.org/10.5194/egusphere-2025-5159
Preprint. Discussion started: 3 December 2025

Ryan, J. C., Smith, L. C., van As, D., Cooley, S. W., Cooper, M. G., Pitcher, L. H., and Hubbard, A.: Greenland Ice Sheet surface melt amplified by snowline migration and bare ice exposure. Sci. Adv., 5, eaav3738, https://doi.org/10.1126/sciadv.aav3738, 2019.

Ryan, J.C., Cooper, M.G., Cooley, S.W. *et al.* Meltwater ponding has an underestimated radiative effect on the surface of the Greenland Ice Sheet. *Nat Commun* **16**, 8274, https://doi.org/10.1038/s41467-025-62503-5, 2025

Sasgen, I., Wouters, B., Gardner, A. S., King, M. D., Tedesco, M., Landerer, F. W., Dahle, C., Save, H., and Fettweis, X.: Return to rapid ice loss in Greenland and record loss in 2019 detected by the GRACE-FO satellites, Communications Earth & Environment, 1, 8, https://doi.org/10.1038/s43247-020-0001-2, 2020.

Selmes, N., Murray, T., and James T. D.: Fast draining lakes on the Greenland ice sheet. Geophys Res Lett, 38, L15501, https://doi. org/10. 1029/2011GL047872, 2011.

Slater, T., Shepherd, A., McMillan, M. Leeson, A., Gilbert, L., Muir, A., Kuipers Munneke, P., Noel, B., Fettweis, X., van den Broeke, M., Briggs, K.: Increased variability in Greenland Ice Sheet runoff from satellite observations. Nat Commun 12, 6069, https://doi.org/10.1038/s41467-021-26229-4, 2021

Sundal, A. V., Shepherd, A., Nienow, P., Hanna, E., Palmer, S., and Huybrechts, P.: Evolution of supra-glacial lakes across the Greenland ice sheet, Remote Sens. Environ., 113(10), 2164–2171, https://doi.org/10.1016/j.rse.2009.05.018, 2009.

Tedesco, M. and Fettweis, X.: Unprecedented atmospheric conditions (1948–2019) drive the 2019 exceptional melting season over the Greenland ice sheet, The Cryosphere, 14, 1209-1223, https://doi.org/10.5194/tc-14-1209-2020, 2020.

Tedesco, M., Willis, I. C., Hoffman, M. J., Banwell, A. F., Alexander, P., and Arnold, N. S.: Ice dynamic response to two modes of surface lake drainage on the Greenland Ice Sheet, Environmental Research Letters, 8, 034007, https://doi.org/10.1088/1748-9326/8/3/034007, 2013

Tedstone, A. and Machguth, H.: Increasing surface runoff from Greenland's firn areas, Nature Climate Change 12, 672–676, https://doi.org/10.1038/s41558-022-01371-z, 2022.

Tedstone, A. J., Bamber, J. L., Cook, J. M., Williamson, C. J., Fettweis, X., Hodson, A. J., and Tranter, M.: Dark ice dynamics of the south-west Greenland Ice Sheet, The Cryosphere, 11, 2491–2506, https://doi.org/10.5194/tc-11-2491-2017, 2017.

Tedstone, A., Machguth, H., Clerx, N. *et al.* Concurrent superimposed ice formation and meltwater runoff on Greenland's ice slabs. *Nat Commun* **16**, 4494 (2025). https://doi.org/10.1038/s41467-025-59237-9

Trusel, L. D., Das, S. B., Osman, M. B., Evans, M. J., Smith, B. E., Fettweis, X., McConnell, J. R., Noël, B. P. Y., and Broeke, M. R. van den: Nonlinear rise in Greenland runoff in response to post-industrial Arctic warming, Nature, 564, 104–108, 2018 https://doi.org/10.1038/s41586-018-0752-4, 2018.

van As, D., Bech Mikkelsen, A., Holtegaard Nielsen, M., Box, J. E., Claesson Liljedahl, L., Lindbäck, K., Pitcher, L., and Hasholt, B.: Hypsometric amplification and routing moderation of Greenland ice sheet meltwater release, The Cryosphere, 11, 1371–1386, https://doi.org/10.5194/tc-11-1371-2017, 2017.

Vandecrux, B., MacFerrin, M., Machguth, H., Colgan, W. T., van As, D., Heilig, A., Stevens, C. M., Charalampidis, C., Fausto, R. S., Morris, E. M., Mosley-Thompson, E., Koenig, L., Montgomery, L. N., Miège, C., Simonsen, S. B., Ingeman-Nielsen,

https://doi.org/10.5194/egusphere-2025-5159
Preprint. Discussion started: 3 December 2025

T., and Box, J. E.: Firn data compilation reveals widespread decrease of firn air content in western Greenland, The Cryosphere, 13, 845–859, https://doi.org/10.5194/tc-13-845-2019, 2019.

Williamson, A. G., Banwell, A. F., Willis, I. C., and Arnold, N. S.: Dual-satellite (Sentinel-2 and Landsat 8) remote sensing of supraglacial lakes in Greenland, The Cryosphere, 12, 3045–3065, https://doi.org/10.5194/tc-12-3045-2018, 2018.

Williamson, A. G., Arnold, N., Banwell, A., and Willis, I.: A Fully Automated Supraglacial lake area and volume Tracking ("FAST") algorithm: Development and application using MODIS imagery of West Greenland, Remote Sens. Environ., 196, 113–133, https://doi.org/10.1016/j.rse.2017.04.032, 2017.

Yang, K., Smith, L. C., Sole, A., Livingstone, S. J., Cheng, X., Chen, Z., and Li, M.: Supraglacial rivers on the northwest Greenland Ice Sheet, Devon Ice Cap, and Barnes Ice Cap mapped using Sentinel-2 imagery, Int. J. Appl. Earth Obs., 78, 1–13, https://doi.org/10.1016/j.jag.2019.01.008, 2019.

Zhang, W., Yang, K., Smith, L. C., Wang, Y., van As, D., Noël, B., Lu, Y., Liu, J.: Pan-Greenland mapping of supraglacial rivers, lakes, and water-filled crevasses in a cool summer (2018) and a warm summer (2019), Remote Sensing of Environment, 297, 113781, https://doi.org/10.1016/j.rse.2023.113781, 2023.